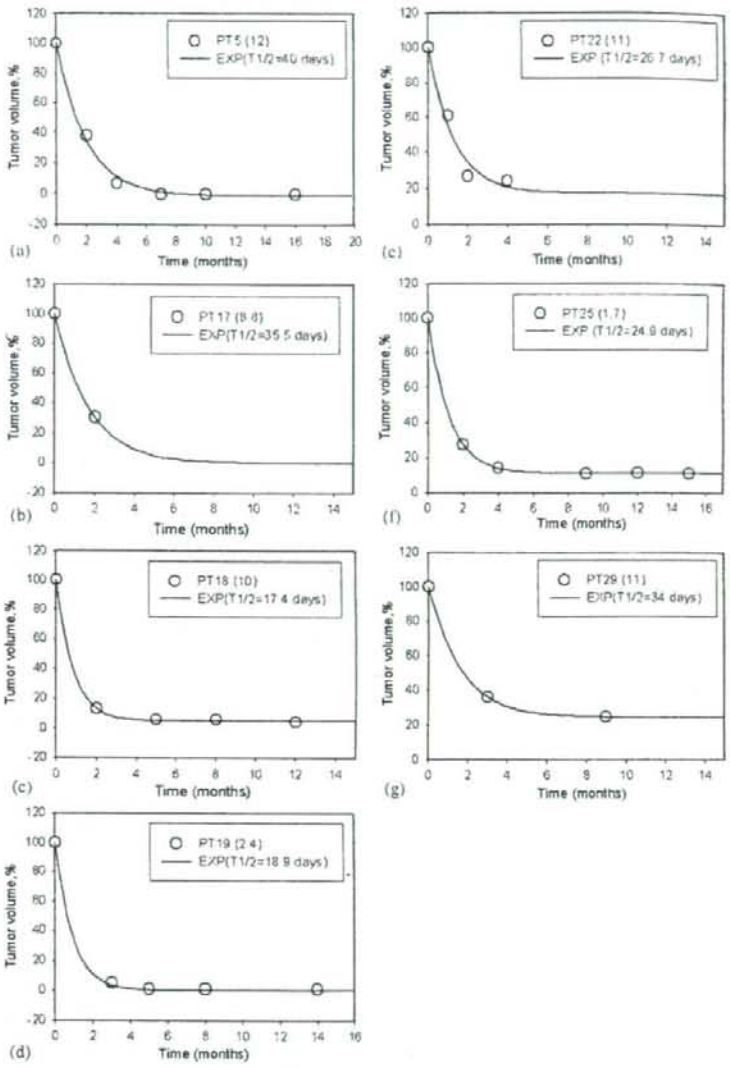

Figure 3. Comparison of the lung squamous cell carcinoma volume after stereotactic body radiotherapy in clinical data of Aoki *et al* with the function $(1-w)\exp(-\ln 2t/T_{1/2})+w$: (a)–(g) patients 1–7. Tumor size (cm^2) is shown for each patient in parentheses.

it suffers radiation damage. The mean life is given by $T_a = T_{1/2}/\ln 2$; therefore, we obtain the average mean life of $T_a = 40.7$ days for SCC and $T_a = 105.5$ days for adenocarcinoma.

The standard deviation of the half-life for both adenocarcinoma and SCC is approximately 30% of the average value. This relatively large value can be explained by several reasons: (1) patient heterogeneity is usually a reason of large standard deviation of radiobiological parameters (Wigg 2001, Keall and Webb 2007); (2) small number of cases in our evaluation

and (3) lung tumors may not be completely reoxygenated at the end of SBRT because this treatment is relatively short; therefore, lethally damaged oxygenated and hypoxic cells may be present in tumors. Hypoxic cells are practically removed from the dividing population of cells in the tumor because they are resting in the Go phase. Hypoxic cells can remain in Go phase for days, weeks or years, but can be stimulated to return to the cell division cycle. Therefore, the disintegration of lethally hypoxic cells may depend on tumor reoxygenation rate and the residual tumor hypoxia may affect heterogeneity of the measured half-life value. According to the data of Rasey *et al* (1996) obtained using PET fluoromisonidazole, the hypoxia for non-small lung cancer can be relatively large with the median value of 47.6% and the maximum value of 94.7%.

4. Discussion

In this paper, we attempted to study the kinetics of the disintegration of tumor cells damaged by radiation and, therefore, unable to proliferate. The radiobiological analysis for radiotherapy treatment planning usually involves the kinetics of proliferating cells because they define the optimal fractionation schedules and treatment outcomes given by TCP and NTCP (Moiseenko *et al* 2005, Stewart and Li 2007). In this radiobiological analysis, a cell is considered instantaneously gone from the system if it is lethally damaged by radiation.

However, the development of new imaging systems has led to more evidence that volumetric tumor changes during radiotherapy can affect tumor dosimetry in highly conformal therapies like proton therapy (Bucci *et al* 2007). Volumetric tumor changes are defined by both proliferating cells and lethally damaged cells which are not able to proliferate. Lethally damaged cells will disintegrate with time and their kinetics will affect the dynamics of tumor mass and volume. The cell loss mechanism has been addressed in the studies discussing tumor growth and its relationship to the potential doubling time and volume doubling time (Fowler 1991). However, quantitative modeling of the tumor volume variation during or after radiotherapy has not been emphasized in radiotherapy treatment planning.

Modeling the volumetric tumor response is a complicated mathematical and radiobiological task because several cell subpopulations should be considered, including proliferating and damaged cells. Many radiobiological processes such as cell survival, reoxygenation, repopulation and reassortment should be modeled. Therefore, we began with the simple task of modeling with a tumor with only one subpopulation, which could be found at the end of the radiotherapy treatment after all living cells were destroyed by ionizing radiation. The tumor at the end of the therapy consisted only of the population of damaged cells which could not proliferate; however, they did make up the bulk of the tumor. These cells disintegrate at the first or a subsequent division after irradiation and their debris is removed.

In this study, we proposed and validated a simple mathematical formula for cell disintegration in tumors treated with ionizing radiation. The parameters of the model have been obtained using clinical data on tumor size variation after stereotactic radiotherapy of solitary lung tumors. To study the cell kinetics based on the volumetric measures, we assumed a linear relationship between the cell number and the tumor volume. We have shown that many complicated processes such as mitotic cell death and diffusion of cell debris can be described as a simple exponential decay. We believe that this model can lead to further development of a fast computational radiobiological model to predict the tumor volume variation during fractionated radiotherapy. To simulate tumor volume during radiotherapy, this model should additionally include an analysis of subpopulations of live cells governed by radiobiological mechanisms such as the LQ survival model, exponential repopulation, reoxygenation and reassortment.

We believe that a radiobiological model for volumetric tumor response is needed for qualitative and quantitative analyses of the most recent clinical results on anatomical changes in the human body during radiation therapy (Barker *et al* 2004, Kupelian *et al* 2005, Siker *et al* 2006, Bucci *et al* 2007). These clinical results indicate that volumetric tumor changes during radiotherapy can affect treatment planning dosimetry for highly conformal radiotherapeutic modalities like IMRT and proton beams. The radiobiological model for volumetric tumor variation can be used in 4D treatment planning for evaluating dose distribution variations which may be due to time-dependent density variations in highly conformal radiotherapeutic modalities like IMRT and proton therapy (Mohan *et al* 2005). The cell disintegration model which we have proposed in this paper can be used in more complicated models for tumor volumetric response during radiotherapy which should include kinetics of living and lethally damaged cells. If these models would be developed they would allow one evaluate dose variations due to time-dependent density variations thus improving 4D treatment planning. The ability to model tumor volume during radiotherapy can especially improve and optimize 4D treatment planning for IMRT and proton therapy, which is a laborious and time-consuming process.

Acknowledgments

This research was partially supported by an Elekta research grant. The authors would like to thank Dr D Siemann and Dr W M Mendenhall for valuable discussions about tumor radiobiology.

References

Aoki T, Nagata Y, Negoro Y, Takayama K, Mizowaki T, Kokubo M, Oya N, Mitsumori M and Hiraoka M 2004 Evaluation of lung injury after three-dimensional conformal stereotactic radiation therapy for solitary lung tumors: CT appearance *Radiology* **230** 101–8

Barker J L *et al* 2004 Quantification of volumetric and geometric changes occurring during fractionated radiotherapy for head-and-neck cancer using an integrated CT/linear accelerator system *Int. J. Radiat. Oncol. Biol. Phys.* **59** 960–70

Bernheim J L, Mendelsohn J, Kelly M F and Dorian R 1977 Kinetics of cell death and disintegration in human lymphocyte cultures *Proc. Natl. Acad. Sci. USA* **74** 2536–40

Borkenstein K, Levegrün S and Peschke P 2004 Modeling and computer simulations of tumor growth and tumor response to radiation therapy *Rad. Res.* **162** 71–83

Bucci M K, Dong L, Liao Z, Chang J, Cox J, Komaki R, Gillin M and Mohan R 2007 Comparison of tumor shrinkage in proton and photon radiotherapy of lung cancer *Int. J. Radiat. Oncol. Biol. Phys.* **63** S686–S7

Byrd R H, Lu P, Nocedal J and Zhu C 1995 A limited memory algorithm for bound constrained optimization *SIAM J. Sci. Comput.* **16** 1190–1208

Chao M, Xie Y, Le Q and Xing L 2007 Modeling the volumetric change of head and neck tumor in response to radiation therapy *Int. J. Radiat. Oncol. Biol. Phys.* **69** S741 (abstract)

Chvetsov A V, Dempsey J F and Palta J R 2007 Optimization of equivalent uniform dose using the L-curve criterion *Phys. Med. Biol.* **52** 5973–84

Clarke G, Collins R A, Leavitt B R, Andrews D F, Hayden M R, Lumsten C J and Mcinnes R R 2000 A one-hit model of cell death in inherited neuronal degenerations *Nature* **406** 195–9

Dionysiou D D, Stamatakos G S, Uzunoglu N K, Nikita K S and Marioli A 2004 A four-dimensional simulation model of tumor response to radiotherapy *in vivo*: parametric validation considering radiosensitivity, genetic profile and fractionation *J. Theor. Biol.* **230** 1–20

Engelsman M and Kooy H M 2005 Target volume dose considerations in proton beam treatment planning for lung tumors *Med. Phys.* **32** 3549–57

Fowler J F 1989 The linear-quadratic formula and progress in fractionated radiotherapy *Br. J. Radiol.* **62** 679–4

Fowler J F 1991 The phantom of tumor treatment—continually rapid proliferation unmasked *Radiother. Oncol.* **22** 156–8

Hall E J and Giaccia A J 2006 *Radiobiology for the Radiologist* 6th edn (Philadelphia: Lippincott, Williams & Wilkins)

Keall P J and Webb S 2007 Optimum parameters in a model for tumor control probability, including interpatient heterogeneity: evaluation of the log-normal distribution *Phys. Med. Biol.* **52** 291–302

Kupelian P A, Ramsey C, Meeks S L, Willoughby T R, Forbes A, Wagner T H and Langen K M 2005 Serial megavoltage CT imaging during external beam radiotherapy for non-small-cell lung cancer: observations on tumor regression during treatment *Int. J. Radiat. Oncol. Biol. Phys.* **63** 1024–28

Mohan R, Zhang X, Wang H, Kang Y, Wang X, Liu H, Ang K K, Kuban D and Dong L 2005 Use of deformed intensity distribution for on-line modification of image-guided IMRT to account for interfractional anatomic changes *Int. J. Radiat. Oncol. Biol. Phys.* **61** 1258–66

Moiseenko V, Deasy J O and Van DyK J 2005 Radiobiological modeling for treatment planning *The Modern Technology of Radiation Oncology. A Compendium for Medical Physicists and Radiation Oncologists* vol 2 ed J Van Dyk (Madison, WI: Medical Physics Publishing) pp 185–220

Rasey J S, Koh W J, Evans M L, Peterson L M, Lewellen T K, Graham M M and Kronh K A 1996 Quantifying regional hypoxia in human tumors with positron emission tomography of [^{18}F] fluoromisonidazole: a pretherapy study of 37 patients *Int. J. Radiat. Oncol. Biol. Phys.* **36** 417–28

Seibert R M, Ramsey C R, Hines J W, Kupelian P A, Langen K M, Meeks S L and Scaperoth D D 2007 A model for predicting lung cancer response to therapy *Int. J. Radiat. Oncol. Biol. Phys.* **67** 601–9

Shibamoto Y and Hara M 2005 Radiobiology of normal lung tissue and lung tumors *Advances in Radiation Oncology in Lung Cancer* ed B Jeremić (Berlin: Springer) pp 59–66

Siker M L, Tome W A and Metha M P 2006 Tumor volume changes on serial imaging with megavoltage CT for non-small-cell lung cancer during intensity modulated radiotherapy: how reliable, consistent, and meaningful is the effect? *Int. J. Radiat. Oncol. Biol. Phys.* **66** 135–41

Spang-Thomsen M, Visfeldt J and Nielsen A 1981 Effect of single-dose X radiation on the growth curves of a human malignant melanoma transplanted into nude mice *Radiat. Res.* **85** 184–95

Stewart R D and Li X A 2007 BGRT: biologically guided radiation therapy—the future is fast approaching! *Med. Phys.* **34** 3739–51

Tannock I and Howes A 1973 The response of viable tumor cords to a single dose of radiation *Radiat. Res.* **55** 477–86

Wigg D R 2001 *Applied Radiobiology and Bioeffect Planning* (Madison, WI: Medical Physics Publishing)

中 咽 頭

永田 靖* 権丈雅浩* 村上祐司* 兼安祐子* 橋本泰年* 藤田 實* 伊藤勝陽*

はじめに

頭頸部癌は，機能温存，形態温存という放射線治療の特徴を最大限に生かせる部位である。特に中咽頭は摂食，構音，嚥下などの重要な機能をもち，大部分の腫瘍が，放射線感受性の高い扁平上皮癌である。以上の点より，中咽頭癌においては，放射線治療が予後改善とQOLの改善に重要な役割を持つ。中咽頭癌に対しては，CDDPを用いた化学放射線療法が一般的であるが，最新のトピックスとしては，1）IMRT（強度変調放射線治療），2）HPV（パピローマウイルス），3）分子標的治療，などが挙げられよう。

① 中咽頭癌について

中咽頭癌のTNM分類は口腔領域癌と同じである（表1）。腫瘍サイズが2cm以内か4cm以内かでT1，T2，T3が分類される。リンパNステージに関しては，他の頭頸部癌と共通である。

表1 中咽頭癌に対するTNM

T1：	<= 2cm
T2：	> 2 to 4cm
T3：	> 4cm
T4：	Adjacent structures
N1：	Ipsilateral single <= 3cm
N2：	Ipsilateral single > 3 to 6cm
	Ipsilateral multiple <= 6cm
	Bilateral, contralateral <= 6cm
N3：	> 6cm

喫煙や飲酒との関連性については従来より指摘されていたが，近年Human papilloma virus（HPV）ウイルスとの関連性が注目されている。

発症年齢的には60～70歳代で最多であり，95%が扁平上皮癌である。

初期症状は局所の疼痛ないしは，頸部リンパ節腫脹である。特に舌根由来では，局所症状が出現しにくいために進行して発見されることや，原発不明頸部リンパ節転移で見つかることが多い。

一般的に予後は，側壁（扁桃）や上壁（口蓋垂，軟口蓋下面）由来が前壁（舌根），後壁由来より良好とされるが，上壁原発の中には66～70Gyの外照射単独で制御困難な症例もある。

頸部リンパ節転移の頻度は，側壁（扁桃）が60～70%で反対側への転移頻度は10～15%である。扁桃由来以外は両側性リンパ節転移が多く，舌根：7～80%，上壁：40～50%，後壁：50～70%である。

放射線治療中の喫煙の悪影響については，Browmanらの報告[1]があり，低酸素による局所制御率の低下はもとより，粘膜炎等の有害事象の悪化は明らかであり，照射期間および前後の禁煙は不可欠である。

② 中咽頭癌に対する放射線治療

1）照射法

中咽頭癌における患者固定の基本はシェル固定である。原則的に下顎を進展させた状態で，口腔内は義歯を外し，可能な限り上顎口腔粘膜を照射範囲よ

* Y. Nagata, M. Kenjyo, Y. Murakami, Y. Kaneyasu, Y. Hashimoto, M. Fujita, K. Ito 広島大学病院放射線治療部
〔索引用語：中咽頭癌〕

表2　全頸部照射領域のCTV

上縁：下顎骨上縁（下顎頭）つまりZygomatic arch上縁（Rouvierを含む）
前上縁ブロック：上顎洞の後部3分の1，口腔の後部3分の1（舌根は十分含む）
下縁：顎下部のできるだけ高位で接合面を作成する。
後縁：副神経節を含む（棘突起後方1～2cm）
前縁：顎下リンパ節を含むが，頭下リンパは顎下リンパ腫大時以外には含まず，口角も外す。 鎖骨上窩については，前後対向2門（前方1門でも可）で照射する。
外側縁：第二肋骨内側縁（肩甲舌骨筋中間腱鎖骨付着部）
下縁：鎖骨下縁（肺ブロックを使用）

り外すためにマウスピースを用いて軽度開口させておく。全頸部照射は，原則として4MVないし6MVのX線を用いた照射法で，half-field照射法を用いる。

線量評価は，原則的には照射野中心で行うが，厚みの異なる広範囲を照射する場合は，2カ所に評価点を分けて，照射することもある。

2）照射野

外照射野の設定の基本原則は，局所病変+領域リンパ節照射である。片側扁桃原発でN0症例以外は，全頸部リンパ領域に予防照射が必要とされる。そのために，一般的には全頸部領域のCTVを40～50Gy照射する。表2に全頸部照射のCTVを，図1と図2に全頸部照射のX線写真での照射範囲を示す。

一般的には全頸部照射の後に，局所病変（照射前のGTV＋1cm）に追加照射するshrinking method法が一般的である。しかし，この局所病変への照射を最初から全頸部照射と同時に行うfield in filed法や，simultaneous integral boost（SIB）技術を用いたIMRT照射法も行われる（図3）。

3）照射線量

中咽頭癌に対する照射線量は，原則的に外照射単独の場合，GTV(primary)に対しては66～70Gy以上の照射線量が必要である。また，GTV（node）（腫大したリンパ節）にも60Gy以上の照射が必要である。そして，CTV領域に対する予防照射線量は，40～50Gy必要である。もし小線源療法が可能な領域は，小線源療法の併用を検討する。GTV（node）には電子線の使用も検討する。もし照射後に明らかに残存した頸部リンパ節には，照射後の手術的郭清も検討が必要である。

3 化学療法との併用

頭頸部癌において放射線治療単独と化学放射線療法とを比較した臨床試験では，おおむね後者の化学放射線療法併用群が局所制御率や生存率で上回ってきた。

Pignonらのmetaanalysisによっても同時化学放射線療法では放射線治療単独と比較して生存延長効果を認めている[2]。

Calaisらは，III～IV期の中咽頭癌を対象とした無作為比較試験においてCBDCA 70mg/m^2＋5FU 600mgの抗癌剤併用により，3年生存が31%より51%，3年局所制御率が42%より66%に向上したとしている[3]。

Denisらも上記臨床試験の最終報告を行い，5年生存が16%より22%に，5年局所制御率が25%より48%に向上したとしている[4]。

以上のように標準的な5年生存率は30～49%で局所制御率は54～85%であるが，国内データとしては日本放射線腫瘍学会（JASTRO）1998年集計結果では，5年原病生存率がI：II：III：IV＝67：63：50：37であり，側壁：上壁：前壁＝57%：62%：35%であった。本年2008年に10年ぶりの最新結果が札幌にて集計される予定である。

4 有害事象

照射中ー照射後56日以内の急性期有害事象には，以下のものがある。

易疲労感，皮膚の発赤・過敏，粘膜炎，嚥下困難・嚥下痛，嗄声，照射野内の一時的な脱毛，味覚・嗅覚の変化，口内乾燥感，体重減少，白血球減少

図1　中咽頭癌におけるX線シミュレータでの照射野（左右方向）

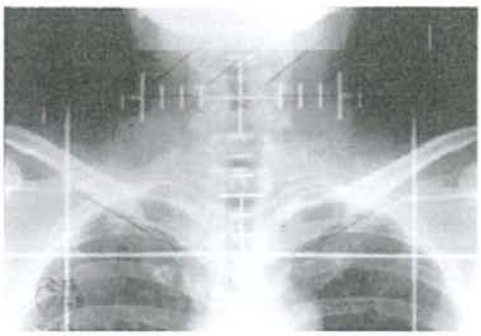

図2　中咽頭癌におけるX線シミュレータでの照射野（前後方向）

照射後57日以後に出現する晩期有害事象として頻度高くみられるものは，以下のものである。

一過性の頸部腫脹（リンパ浮腫），口内乾燥，う歯・歯牙脱落

頻度の少ない晩期有害事象として，照射野内の皮膚の肥厚，永続的な皮膚の色素沈着，頸の筋肉の炎症，永続性の頸部腫脹，聴覚障害，眼障害による失明，鼻腔からの排液・出血，味覚・嗅覚の変化，甲状腺機能低下（特に全頸部照射症例），脊髄障害（軽度のLhermitte徴候），骨・軟骨壊死，筋肉障害による咀嚼，発語，嚥下困難，放射線誘発癌，脊髄麻痺，脳壊死，がある。

5 術後照射

術後照射の適応は，一般的に以下の条件を一つでも満たした症例に対して行われる。

複数リンパ節転移陽性例，リンパ節節外浸潤陽性例，断端陽性例，悪性組織例（undifferentiated cellなど）

術後照射の照射野は，疾患と症例に応じて，また手術時所見によって設定されることが多いが，全頸部照射野か部分頸部照射野が設定される。

現在の術後照射線量は50Gy/2Gyが原則であるが，手術時所見に応じて60Gyまで照射することがある。脊髄線量は40～46Gy以内に制限する。なお術後照射は手術手技による影響が多大であるために，照射野決定前に必ず耳鼻科・放射線治療科カンファレンスで，術者の意向を聴取しておくことが望ましい。また，術後照射も可能な限り，抗癌剤併用が望ましい。

6 HPVウイルスとの関連

最近の研究[5,6]によると頭頸部癌におけるHPVウイルスの感染頻度は有意に高く，特に中咽頭が35.6%，口腔癌が23.5%，喉頭癌が24%とされる。この中で特にHPV16のサブタイプが最も高頻度であり，各々86.7%，68.2%，68.2%であった。中咽頭癌の中では扁桃原発が特にHPVとの関連性が高いとされる。またオラルセックスとの関連性も指摘されている。将来的にHPVワクチンがこれらの癌予防に役立つ可能性がある。

7 IMRT（強度変調放射線治療）

原則的にはターゲットとしてGTV-primary（MRI

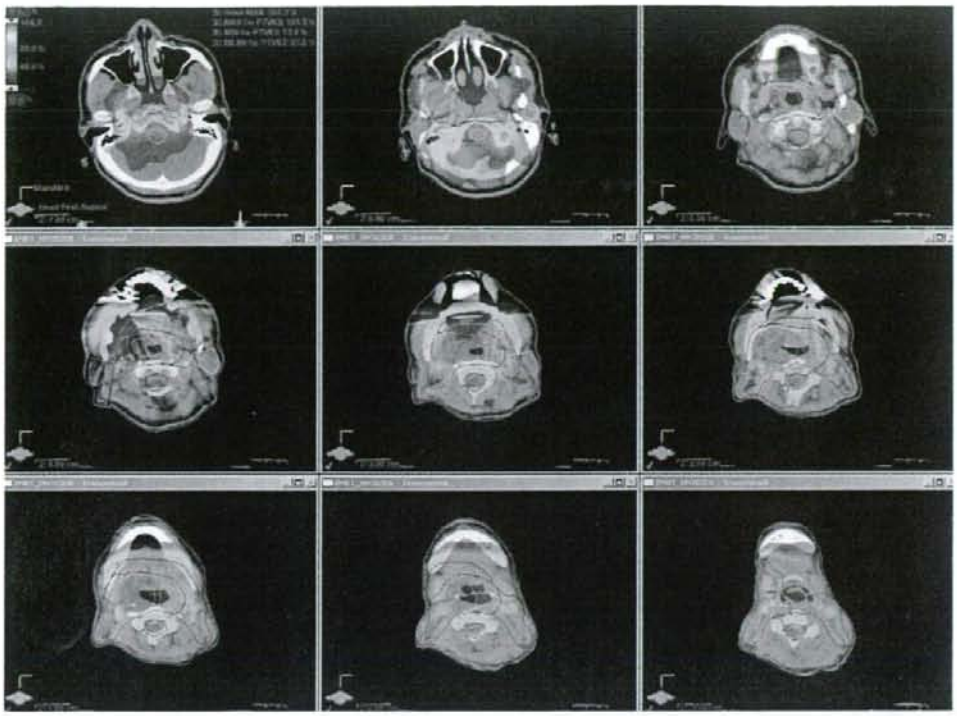

図3　中咽頭癌に対するIMRT（IMRTによる線量分布）

で確認できる肉眼的原発巣）とGTV-node（MRIやPETで確認できる転移腫大リンパ節）とCTV（ルビエールからII-VIの領域リンパ節）を入力するとともに，脊髄，脳幹，唾液腺，喉頭等のリスク臓器との相関で最適線量を決定する。近年はHigh risk PTV，Intermediate risk PTV，Standard risk PTVを決める方法もある。IMRTに関しては腫瘍のGTVと共に特にCTVリンパ領域の輪郭入力[7]が不可欠である。これらのリンパ領域については，RTOG（http://www.rtog.org/hnatlas/main.html）やEORTCのホームページで公開されているために，これらを利用したい。

中咽頭癌に対するIMRTはRTOG：H00-22が既に登録終了し，解析された。このH00-22プロトコールではT1-2 N0-1の中咽頭癌が対象となっている。放射線治療単独であるが，GTVには66Gy/30fx，CTVには54～60Gy/30fxを照射している。参考にRTOG02-25の上咽頭プロトコールではGTV 70Gy/33fx，CTV 59.4Gy/33fxとなっている。また正常組織に関する線量制約においても，PTV 66 95%，PTV 50 95%の他に，耳下腺は30Gyが50%以下または平均線量が26Gy以下，脊髄は最大線量45Gy以下，脳幹では54Gy以下，その他の領域では72.6Gy以下としている。

H00-22のASTRO 2006における中間解析[8]では線量制約において完全にプロトコールを遵守できた患者はいなかったという（89%がminor deviation，11%がmajor variation）。急性期有害事象としては口内乾燥感（Xerostomia）：grade 2 49.3%，grade 3 1.5%（conventional RTではgrade 2～3 84%），口内粘膜炎（Mucositis）：grade 2 29.9%，grade 3 25.4%，grade 4 1.5%，頸部皮膚炎（Skin）：grade 2 19.4%，grade 3 10.4%，顎骨壊死（Osteoradionecrosis）：grade 2～4 6.2%で

あった。平均観察期間1.6年の時点で67人照射中3人の局所再発がみられている。2008年ASTRO（#219）の最終報告でも，唾液腺機能温存が証明された。

Chaoらは，文献9で74人の初期経験を報告し，4年局所制御率が87%でありまた4年全生存率も87%としている。この中でGTV特にGTV-LNの設定が重要としている。

De Arrudaらも，文献10で50人の治療経験で2年局所無再発率が98%，2年無遠隔転移率が84%としている。

Leeらも文献11において20カ月以上観察された症例において，grade 2以上の口内乾燥症状が67%より12%に有意に低下したとしている。

上記いずれのIMRT報告においても，有害事象の発生率は従来法より明らかに低い。ただ，IMRTが生存率改善に直結しているかについてはHodgeらはIMRT以外の要素の影響があり結論できないとしている[12]。

8 分子標的治療

頭頸部癌においても，分子標的治療の有用性が報告されるようになってきた。最近の臨床試験においては，Bonnerらが文献13またPfisterらが文献14において，Cetuximab：C225が放射線治療と併用することによって，有意に局所無再発生存期間，無増悪期間，全生存期間が改善するとされた。わが国においても大腸癌に引き続くErbituxの臨床適応拡大が期待される。

おわりに

IMRTの導入により従来より明らかに有害事象の軽減した根治照射が可能となってきた。また化学療法の併用で治療成績が向上し，新たな分子標的治療の併用も期待される。現在にわが国において中咽頭癌は手術と放射線治療との境界領域であるが，今後は患者への負担の少ない放射線治療の意義が改めて見直されるべき時であろう。

文　献

1) Browman GP et al：Influence of cigarette smoking on the efficacy of radiation therapy in head and neck cancer. NEJM 328：159-163, 1993
2) Pignon JP et al：Chemotherapy adds to locoregional treatment for head & neck squamous cell carcinoma. Lancet 355：949-955, 2000
3) Calais G et al：Randomized trial of radiation therapy versus concomitant chemotherapy and radiation therapy for advanced-stage oropharynx carcinoma. JNCI 91：2081-2086, 1999
4) Dennis F et al：Final results of the 94-01 French Head and Neck oncology and radiotherapy group randomized trial comparing radiotherapy alone with concomitant radiochemotherapy in advancedstage oropharynx carcinoma. JCO 22：69-76, 2004
5) D'Souza et al：Case-control study of human papillomavirus and oropharyngeal cancer. NEJM 356：1944-1956, 2007
6) Syrjanen S et al：Human papillomaviruses in head and neck carcinoma. NEJM 356：1993-1995, 2007
7) Gregoire V et al：CT-based delineation of lymph node levels and related CTVs in the node-negative neck. DAHANCA, EORTC, GORTEC, NCUC, RTOG consensus guidelines. Radiother Oncol 69：227-236, 2003
8) Eisbuch A et al：Phase II multi-instituional study of IMRT for oropharyngeal cancer（RTOG 00-22）. Early results. IJROBP 66：S46, 2006
9) Chao C et al：IMRT for oropharyngeal carcinoma：impact of tumor volume. IJROBP 59：43-50, 2004
10) De Arruda et al：IMRT for the treatment of oropharyngeal carcinoma：The Memorial Sloan-Kettering Cancer Center experience. IJROBP 64：363-373, 2006
11) Lee NY et al：A comparison of IMRT and concomitant boost radiotherapy in the setting of concurrent chemotherapy for locally advanced oropharyngeal carcinoma. IJROBP 66：966-974, 2006
12) Hodge CW et al：Are we influencing outcomes in oropharyngeal carcinoma with IMRT? An inter-era comparison. IJROBP 69：1032-1041, 2007
13) Bonner JA et al：Radiotherapy plus Cetuximab for squamous cell carcinoma of the head and neck. NEJM 354：567-578, 2006
14) Pfister DG et al：Concurrent Cetuximab, Cisplatin and Concomitant Boost Radiotherapy for Locoregional advanced squamous head and neck cancer. JCO 24：1072, 2006

Radiotherapy and Oncology xxx (2009) xxx–xxx

Contents lists available at ScienceDirect

Radiotherapy and Oncology

journal homepage: www.thegreenjournal.com

Original article

Dose–response relationship and dose optimization in radiotherapy of postoperative keloids

Takashi Sakamoto [a,b,*], Natsuo Oya [a,b], Keiko Shibuya [b], Yasushi Nagata [b], Masahiro Hiraoka [b]

[a] Department of Radiation Oncology, Kumamoto University, Japan
[b] Department of Radiation Oncology and Image-applied Therapy, Kyoto University, Japan

ARTICLE INFO

Article history:
Received 18 November 2007
Received in revised form 30 December 2008
Accepted 31 December 2008
Available online xxxx

Keywords:
Postoperative keloid
Irradiation therapy
Radiotherapy
Dose relationship
Dose optimization

ABSTRACT

Background and purpose: The treatment dose and fractionation dose that are considered in postoperative keloids had been reported in the previous studies. We performed retrospective analysis to elucidate the factors influencing the treatment outcome.

Materials and methods: From 1979 to 1994, 194 lesions in 119 patients received postoperative radiotherapy after excision with the total dose ranging from 16 Gy/8 fr to 40 Gy/8 fr (mean: biologically effective dose (BED) 33.5 Gy). Kilo-voltage X-rays (55 or 100 kVp) or electron beams (4 or 6 MeV), including entire keloid scars, and any suture/puncture holes with a margin around the lesion were used. The median follow-up period was 36 months (range 12–164 months).

Results: Symptomatic pain and itching relief were achieved in 96% and 91%, respectively. The relapse rate was 11% at 20 Gy in five fractions or higher dose, while 43% at less than 20 Gy. On the other hand, the incidence of adverse effects was significantly higher for patients receiving more than 20 Gy in five fractions.

Conclusion: There was a significant correlation between the relapse rate and the total dose of irradiation, and between adverse effects and the total dose. To correlate local control and adverse effects, we proposed 20 Gy in five fractions as the optimal dose for the postoperative of keloids. A significant correlation between relapse rate and the interval time between excision and radiotherapy was not found in our current study.

There is no universally effective treatment method for keloids and hypertrophic scars. The recurrence rates after surgical excision alone vary from 50% to 80%, thus leading to the development of many adjuvant therapeutic modalities [1]. Several therapeutic techniques have been tested, including continuous pressure after surgery, corticosteroid injections [2], carbon dioxide laser [3], NdYaG laser [4], silicone gel [5], retinoic acid [6], and silastic sheet coverage [7]. However, these methods seem unsatisfactory for preventing keloid recurrence; the recurrence rate is reported to be above 50%.

The value of radiation therapy in the treatment of keloids has been known for many years. In a randomized trial, Sclafani et al. [8] observed a higher recurrence of keloids after surgery and steroid injections than after surgery and radiotherapy. After the total excision of keloids and hypertrophic scars, radiation therapy has been demonstrated as one of the most effective treatment methods to prevent recurrence, showing a recurrence rate around 20% [9–12].

In this study, we reviewed keloids treated with postoperative radiotherapy in our hospital, and retrospectively analyzed in regard to long-term control, symptomatic relief and adverse effects to elucidate the factors influencing the treatment outcome.

Materials and methods

Patients

From September 1979 to July 1994, 194 lesions in 119 patients received postoperative radiotherapy at Kyoto University Hospital. The characteristics of the patients and lesions are summarized in Tables 1 and 2. All patients were Asian, 35 men and 84 women, aged 4–75 years with a median age of 25 years. Fifty-seven of the 194 lesions had been treated previously with surgical excision and/or local steroid injection, but none had received radiotherapy previously.

Treatment methods

The treatment parameters are summarized in Table 3. Various dose schedules were used, with the total dose ranging from

* Corresponding author. Address: Department of Radiation Oncology, Graduate School of Medical Sciences, Kumamoto University, 1-1-1 Honjo, Kumamoto 860-8556, Japan.
E-mail address: stakashi@kumamoto-u.ac.jp (T. Sakamoto).

0167-8140/$ - see front matter © 2009 Published by Elsevier Ireland Ltd.
doi:10.1016/j.radonc.2008.12.018

Table 1
Characteristics of 119 patients.

	Number of patients
Sex	
Male	35
Female	84
Age	
<10	3
10–19	32
20–29	44
30–39	10
40–49	10
50–59	10
60–69	5
70≤	5
Median (range) 25 (4–75)	
Keloid lesions	
1	84
2	19
3	5
4	6
5	1
6	2
7	1
12	1
Median (range) 1 (1–12)	
Total	119

Table 2
Characteristics of 194 keloids.

	Number of keloids
Previous treatment	
(−)	137
(+)	57
Size (cm)	
<2.0	10
2.0–3.9	44
4.0–5.9	34
6.0–7.9	26
8.0–9.9	23
10.0–14.9	26
15.0–19.9	17
20≤	14
Site	
With high stretch tension	149
Sternum	68
Shoulder	40
Chest wall	23
Arm	11
Back	7
Without high stretch tension	45
Neck	15
Upper abdomen	11
Lower abdomen	10
Ear	4
Lower limbs	4
Face	1
Etiology	
Minor stimulations	109
Acne	44
Varicella	16
Vaccination	15
Insect wound	7
Herpes	1
Unknown	26
Major stimulations	85
Surgery	48
Burn	17
Trauma	17
Abscess	5
Total	194

16 Gy in 8 fractions to 40 Gy in 8 fractions. The total treatment time ranged from 5 days to 47 days, with a median of 9 days. The interval from excision to irradiation ranged from 1 day to 72 days, with a median of 7 days. Four fractions of 4 Gy in 8–10 days were the most common treatment schedule for postoperative radiotherapy.

In most cases, either 55 kVp (10 mA, 1.0 mm Be and 0.78 mm Al filters) or 100 kVp (8 mA, 1.0 mm Be and 1.7 mm Al filters) X-ray at a dose rate of 1–11 Gy/min was used. For only six lesions, 4 or 6 MeV electron beams were used. The choice of radiation source depended on the height, size, and position of the lesion. The 90% isodose target area included the entire postoperative scar and any suture/puncture hole with a margin of 1–5 mm around the lesion. Non-target areas were shielded by an individually cut 1–2 mm lead sheet.

Evaluation of treatment response and adverse effect

The initial response to treatment was evaluated in all 194 lesions at the first follow-up examination (1–6 months after the end of radiation treatment). Symptomatic relief was assessed if the lesion had caused pain and/or itching before treatment. A judgment of recurrence was made when the height of a lesion began to increase even just a little.

The existence of moderate to severe skin hyperpigmentation and/or telangiectasis with depigmentation was regarded as a positive adverse effect. Mild or transitory pigmentation, which disappeared within a year after treatment and did not affect cosmesis, was not regarded as a positive adverse effect.

Our follow-up policy for patients with keloids consists of a 6-month observation for at least 2 years after radiotherapy. We used telephone interviews for some patients who could not visit our hospital. All keloids were enrolled in the present study were followed up for 12 months or longer. The follow-up time ranged from a minimum of 12 months to a maximum of 164 months, with a median follow-up of 36 months.

Statistical analysis

In long-term recurrence rate and the positive adverse effect rate, univariate analysis using the logrank test and multivariate analysis using the Cox proportional hazard model were performed with the following factors: gender, patient age, involved site, etiology, keloid size, previous treatment, affliction time, interval from excision, source of radiation, and total dose. Various dose schedules were used, instead of the total dose, so we calculated biologically effective dose (BED) according to Kal et al. [13]. All calculations were with Stat View J 5.0 software (SAS Institute Inc, Chicago, IL). Differences with a *p-value* of less than 0.05 were considered statistically significant.

Results

Symptomatic relief is summarized in Table 4. Itching and pain relief was achieved in 91% and 96% of symptomatic keloids, respectively.

We calculated BED according to Kal et al. [13], and plotted the control rates as a function of BED. We showed a dose–response relationship in Fig. 1a. Long-term recurrence rates of postoperative keloids are shown in Fig. 1b. At 36 months, 64 of 194 keloids treated with excision and radiotherapy had relapsed (33%). The univariate and multivariate analyses are shown in Table 5. Univariate analysis showed that the recurrence rate was significantly higher

Please cite this article in press as: Sakamoto T et al. Dose–response relationship and dose optimization in radiotherapy ... Radiother Oncol (2009), doi:10.1016/j.radonc.2008.12.018

Table 3
Treatment methods of 194 keloids.

	Number of fractions	Number of keloids
Fraction dose (Gy)		
2	8	3
2	10	5
2	13	4
2	20	2
2.5	8	1
2.5	10	1
2.5	14	1
3	6	1
3	10	13
3	12	1
3	13	1
4	4	128
4	5	4
4	6	24
5	4	1
5	5	1
5	6	2
5	8	1
Radiation source		
X-ray		
55 kVp		74
100 kVp		114
Electron		
4 MeV		4
6 MeV		2
Total treatment time (days)		
5–9		106
10–14		47
15–19		11
20–24		9
25–29		12
30–34		2
35–39		5
40≤		2
Median 9 days		
Interval between operations and irradiations (days)		
<2		22
2–5		66
6–9		33
10–14		37
15–19		14
20–24		5
25–29		12
30≤		5
Median 7 days		
Total		194

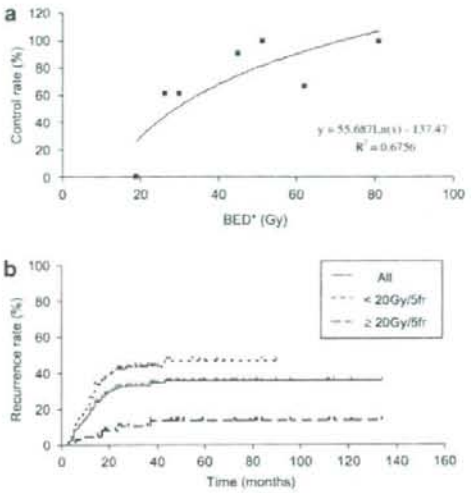

Fig. 1. (a) Control rate of keloids as function of the biologically effective dose (BED). There was a significant correlation between the control rate and biologically effective dose (BED*). *BED calculation according to Kal et al. [13]. (b) Long-term recurrence rate in post-operative radiotherapy according to the total dose. The recurrence rate ≥20 Gy in five fractions was significantly lower than that with <20 Gy in five fractions. **Significant (logrank test).

for doses lower than 20 Gy in five fractions and for women. In multivariate analysis, these factors remained significant.

The positive adverse effect rate was 19% (36/194) in all lesions, and univariate and multivariate analyses of adverse effect rate are shown in Table 6. Univariate analysis showed that the adverse effect rate was significantly higher for elderly patients (≥25 years old), minor etiology, large keloids (longer axis ≥5 cm), previous treatment, use of high voltage X-rays (100 kVp) or electrons, and total dose of 20 Gy in five fractions or higher. In multivariate analysis, the factors of elderly patients, minor etiology, and of previous treatment remained significant.

There were no cases of serious toxicity, defined as World Health Organization grade 3 or higher. There were no cases of malignant tumors being generated at the keloid site.

Table 4
Symptomatic relief.

Symptomatic relief	Pain lesions (%)	Itching lesions (%)
None	116	65
Relief	75/78 (96)	118/129 (91)
No change	3/78 (4)	11/129 (9)
Worse	0	0
Total	194	194

Discussion

Consistent reliable control of keloids using postoperative irradiation has been reported by many authors [10–12,14–18]. There is a controversy concerning the total dose in these previous reports, as well as whether the treatment was given in one fraction or in several fractions. There was no consensus with respect to the total dose and dose fractionation in the treatment of keloids. A summary of the local control rates of postoperative radiotherapy of keloids is shown in Table 7 [1,10–12,14,19–27].

The mechanism of the radiotherapeutic prevention of keloids is still poorly understood. One of the proposed mechanisms is the control of collagen synthesis by eliminating abnormally activated fibroblasts and promoting the existing normal fibroblasts [28]. In vitro experimental evidence suggests that a fraction dose of about 5 Gy may be effective in inducing radiolysis of fibroblasts [18]. Using in vivo experiments with rat skin, the radiolytic process of fibroblasts starts minimally from 0.5 to 2.5 Gy. Recoiled collagen fibrils return to their normal shape and size 4–6 weeks after radiotherapy [18].

However, a higher dose seems necessary in the clinical situation. Brown and Bromberg identified a minimum isoeffect time–dose line for reliable postoperative keloid control at 9–10 Gy delivered over 1 week or 15 Gy over 2 weeks. With BED above this level, 100% control was achieved [29]. Edsmyer et al. confirmed the threshold dose for reliable control as 12–14 Gy in single fraction by X-ray in the postoperative setting and it is

Please cite this article in press as: Sakamoto T et al. Dose–response relationship and dose optimization in radiotherapy ... Radiother Oncol (2009), doi:10.1016/j.radonc.2008.12.018

Table 5
Long-term control of 194 keloids.

Factor	Category (n)	Recurrence rate (%)	Univariate analysis	Multivariate analysis
Gender	Male (85)	25	$p = 0.031^{*}$	$p = 0.0069^{**}$
	Female (109)	39		
Age	<25 y.o. (132)	38	$p = 0.083$	$p = 0.42$
	⩾25 y.o. (62)	23		
Site	Without high tension (45)	29	$p = 0.48$	$p = 0.50$
	With high tension (149)	34		
Etiology	Minor (109)	37	$p = 0.23$	$p = 0.075$
	Major (85)	28		
Longer axis	<5 cm (74)	36	$p = 0.53$	$p = 0.75$
	⩾5 cm (120)	31		
Previous treatment	− (137)	32	$p = 0.62$	$p = 0.97$
	57	35		
Affliction time	<5 years (73)	38	$p = 0.17$	$p = 0.063$
	⩾5 years (121)	30		
Interval from operation	<6 days (88)	34	$p = 0.83$	$p = 0.62$
	⩾6 days (106)	32		
Source	55 kvp (74)	37	$p = 0.54$	$p = 0.15$
	100 kvp, electron (120)	31		
Total dose	<20 Gy (132)	43	$p < 0.0001^{*}$	$p = 0.0002^{**}$
	⩾20 Gy (62)	11		

* Significant (logrank test).
** Significant (Cox proportional hazard model).

probably best to give the radiotherapy immediately after the excision [24,30]. Van den Brenk et al. reported that possible skin necrosis after single-fraction irradiation encouraged fractionated radiotherapy schedules, regardless of the dose [31]. According to Kal et al. [13], biologically effective doses (BEDs) of the various irradiation regimens were calculated using the linear–quadratic concept, and the recurrence rate decreased as a function of BED in the range of BED above 20 Gy. At a BED higher than 20 Gy, the recurrence rate was lower than 10%.

Thus, the dose–response relationship in the treatment of postoperative keloids had been reported in several previous studies. Also, in our study, we found a significant correlation between the recurrence rate and the total dose. The recurrence rate was 11% at a total dose of 20 Gy in five fractions or higher, while 43% under 20 Gy in five fractions. The recurrence rate was 33% for all lesions evaluated in this study, which was comparable to that of the previous studies (Table 7); however, the recurrence rate for lesions treated with the schedule of 20 Gy in five fractions, equivalent to a BED of 30 Gy according to Kal et al. [13], was 18%. It was suggested that this dose fraction was necessary and sufficient for keloid control. On the other hand, the positive adverse effect rate was also dose-dependent; 44% at a total dose of 20 Gy in five fractions or higher, while 7% at under 20 Gy; however, the positive adverse effect rate for the schedule of 20 Gy in five fractions was

Table 6
Adverse effects of 194 keloids.

Factor	Category (n)	Adverse effect (%)	Univariate analysis	Multivariate analysis
Gender	Male (85)	22	$p = 0.30$	$p = 0.56$
	Female (109)	16		
Age	<25 y.o. (132)	13	$p = 0.0057^{*}$	$p = 0.0018^{**}$
	⩾25 y.o. (62)	31		
Site	Without high tension (45)	11	$p = 0.092$	$p = 0.61$
	With high tension (149)	21		
Etiology	Minor (109)	26	$p = 0.0047^{*}$	$p = 0.032^{**}$
	Major (85)	9		
Longer axis	<5 cm (74)	9	$p = 0.041^{*}$	$p = 0.64$
	⩾5 cm (120)	24		
Previous treatment	−(137)	24	$p = 0.0071^{*}$	$p = 0.0089^{**}$
	+(57)	5		
Affliction time	<5 years (73)	12	$p = 0.25$	$p = 0.33$
	⩾5 years (121)	22		
Interval from operation	<6 days (88)	24	$p = 0.53$	$p = 0.70$
	⩾6 days (106)	15		
Source	55 kvp (74)	5	$p = 0.0037^{*}$	$p = 0.13$
	100 kvp, electron (120)	27		
Total dose	<20 Gy (132)	7	$p < 0.0001^{*}$	$p = 0.039^{**}$
	⩾20 Gy (62)	44		

* Significant (logrank test).
** Significant (Cox proportional hazard model).

Please cite this article in press as: Sakamoto T et al. Dose–response relationship and dose optimization in radiotherapy ... Radiother Oncol (2009), doi:10.1016/j.radonc.2008.12.018

Table 7
Summary of local control rates of post-operative radiotherapy of keloids.

Author (Year)	Number of cases	Median follow-up time (months)	Treatment dose (Gy)	Number of fraction	Radiation type	Interval between operation and irradiation (days)	Local control rate (%)	BED (Gy)
Cosman (1961)	94	12	7.7*	4	Deep X	14–42	69	10.6*
Craig (1965)	16	12	7.7*	1	100 kVX	<2	87	16.2*
King (1970)	32	Unknown	9.6–28.8	1–3	1–3 MeV–E	<1	74.1	Mean 29.7*
Mathangi-Ramakrishan (1974)	36	Unknown	15.4*	2–3	Deep X	<1	98	Mean 34.7*
Edsmyr (1975)	103	2	4.8–23*	1–14	45,100 kVX	<8	80	Mean 28.6*
Levy (1976)	35	6	14.4–17.3*	5–6	100 kVX	1–2	88	Mean 23.8*
Ollstein (1981)	68	12	14.4*	3	100 kVX	<1	79	25.1*
Enhamre (1983)	62	6	9.6–14.4*	1–3	20 kVX	1–14	88	Mean 32.7*
Borok (1988)	375	Unknown	3.8–15.4*	Variety (3–4***)	X, E	<2**	97.6	15.9–21.3***
Kovalic (1989)	113	117	3–20	1–5	X 89% Co, E 11%	1–21	73	Mean 18.8
Doornbos (1990)	263	12	4.5–18	2–4	120 kVX	3–10	85.7***	24.1***
Escarmant (1993)	570	15	8–30	1	LDR	<2	79	Mean 55.8
Norris (1995)	24	24	8–12*	1–3	E 5 100 kV X 19	1–68	47	Mean 17.8
Ogawa (2003)	14	24	15	3	4 MeV–E	<2	67	22.5
Current study	194	36	16–40	4–20	55, 100 kVX 188 4, 6 MeV-E 6	1–72 (mean 9.7)	67	Mean 33.5

LDR, low dose rate 192Ir; X, X-ray beam; E, electron beam; Co, cobalt beam.
* For BED calculation we applied 1R = 0.96 cGy.
** After 1981, radiation technique was standardized to 1200–1600 rad in three to four fractions.
*** 15 Gy in three fractions.

not very high (18%). Thus, we considered this dose fraction to be acceptable regarding morbidity. Therefore, since 1995, we have employed a schedule of 20 Gy in five fractions for almost all newly treated postoperative keloids, in the expectation of preserving low morbidity without compromising the control rate.

In the prognostic analysis of this study, female gender was associated with a higher recurrence rate. Previous studies had scarcely demonstrated a correlation between gender and recurrence. The cure of hypertrophic scars is occasionally protracted in young women, maybe because the propagation of fibroblasts is exceeded during recovery at the wound [32,33]. In addition, elderly patients and previous treatment were associated with a higher positive adverse effect rate. Aging and treatment history may cause potentially enhanced radiosensitivity of normal cutaneous tissue, possibly resulting in greater adverse effects.

The influence of the interval between excision and the commencement of radiotherapy on recurrence remains controversial. Cosman et al. [1,34] and Hintz [35] suggested an advantage of the rapid initiation of postoperative irradiation. In contrast, Enhamre and Hammar [36] found no association with the results and interval time between excision and irradiation. In our study, we did not find a significant correlation between the recurrence rate and the interval between excision and radiotherapy, possibly because its influence may have been masked by the large variation of the dose fractionation. This should be further studied using a uniform dose fractionation schedule.

The total radiation dose correlated significantly both with the recurrence rate and with the positive adverse effect rate. It was suggested that 20 Gy in five fractions was a recommendable dose fractionation schedule in the expectation of preserving low morbidity without compromising the control rate.

Acknowledgement

The authors sincerely thank Professor Shigehiko Suzuki, Department of Plastic Surgery, Kyoto University Hospital, for his professional advice concerning the practice of surgery for keloids.

References

[1] Cosmann B, Crikelar GF, Ju DMC, Gaulin JC, Lattes R. The surgical treatment of keloids. Plas Reconstr Surg 1961;27:335–58.
[2] Kiil J. Keloids treated with topical injections of triamcinolone acetonide. Scand J Plast Reconstr Surg 1977;11:169–72.
[3] Apfelberg DB, Maser MR, White DN, Lash H. Failure of carbon dioxide laser excision of keloids. Lasers Surg Med 1989;9:382–8.
[4] Sherman R, Rosenfeld H. Experience with the Nd YAG laser in the treatment of keloid scars. Ann Plast Surg 1988;21:231–5.
[5] Mercer NS. Silicone gel in the treatment of keloid scars. Br J Plast Surg 1989;42:83–7.
[6] Panabiere-Cataing MH. Retinoic acid in the treatment of keloids. J Dermatol Surg Oncol 1988;14:1275–6.
[7] Ohmori S. Effectiveness of silastic sheet coverage in the treatment of scar keloid (hypertrophic scar). Aesthetic Plast Surg 1988;12:95–9.
[8] Sclafani AP, Gordon L, Chadha M, et al. Prevention of earlobe keloid recurrence with postoperative corticosteroid injections versus radiation therapy: a randomized, prospective study and review of the literature. Dermatol Surg 1996;22:569–74.
[9] Guix B, Henriquez I, et al. Treatment of keloids by high-dose-rate brachytherapy: a seven-year study. Int J Radiat Oncol Biol Phys 2001;50(1):167–72.
[10] Borok TL, Bray M, Sinclair I, et al. Role of ionizing irradiation for 393 keloids. Int J Radiat Oncol Biol Phys 1988;15:865–70.
[11] Kovalic JJ, Perez CA. Radiation therapy following keloidectomy: a 20-year experience. Int J Radiat Oncol Biol Phys 1989;17:77–80.
[12] Escarmant P, Zimmermann S, Amar A, et al. The treatment of 783 keloid scars by iridium 192 interstitial irradiation after surgical excision. Int J Radiat Oncol Biol Phys 1993;26:245–51.
[13] Kal HB, Veen RE. Biologically effective dose of postoperative radiotherapy in the prevention of keloids. Strahlenther Onkol 2005;181:717–23.
[14] Doornbos JF, Stuffel TJ, Hass AC, et al. The role of kilovoltage irradiation in the treatment of keloids. Int J Radiat Oncol Biol Phys 1990;18:833–9.
[15] Clavere P, Bedane C, Bonnetblanc JM, et al. Postoperative interstitial radiotherapy of keloids by iridium 192: a retrospective study of 46 treated scars. Dermatology 1997;195:349–52.
[16] Caccialanza M, Piccinno R, Schiera A. Postoperative radiotherapy of keloids: a twenty-year experience. Eur J Dermatol 2002;12:58–62.
[17] Dinh Q, Veness M, Richards S. Role of adjuvant radiotherapy in recurrent earlobe keloids. Australas J Dermatol 2004;45:126–62. Q3
[18] Malaker K, Vijayraghavan K, Hodson I, et al. Retrospective analysis of treatment of unresectable keloids with primary radiation over 25 years. Clin Oncol (R Coll Radiol) 2004;16:290–8.
[19] Norris JE. Superficial X-ray therapy in keloid management: a retrospective study of 24 cases and literature review. Plast Reconstr Surg 1995;95:1051–5.
[20] Cohen IK, Peacock EE. Keloids and hypertrophic scars. In: McCarthy JG, editor. Plastic surgery. Philadelphia: W.B. Saunders Company; 1990. p. 732–47.
[21] Craig RDP, Pearson D. Early post-operative irradiation in the treatment of keloid scars. Br J Plast Surg 1965;18:369–76.
[22] King GD, Salzman FA. Keloid scars; analysis of 89 patients. Surg Clin North Am 1970;50:595–8.
[23] Mathangi-Ramakrishnan K, Thomas KP, Sundararajan CR. Study of 1000 patients with keloids in South India. Plast Reconstr Surg 1974;53:276–86.
[24] Edsmyr F, Larsson LG, Onyango J, et al. Radiotherapy in the treatment of keloids in East Africa. East Afr Med J 1973;50:457–61.
[25] Levy DS, Salter MM, Roth RE. Postoperative irradiation in the prevention of keloids. Am J Roentgenol 1976;127:509–10.
[26] Ollstein RN, Siegel HW, Gillooley JF, et al. Treatment of keloids by combined surgical excision and immediate post-operative X-ray therapy. Ann Plast Surg 1981;7:281–5.

Please cite this article in press as: Sakamoto T et al. Dose–response relationship and dose optimization in radiotherapy ... Radiother Oncol (2009), doi:10.1016/j.radonc.2008.12.018

[27] Ogawa R, Mitsuhashi K, Hyakusoku, et al. Postoperative electron-beam irradiation therapy for keloids and hypertrophic scars: retrospective study of 147 cases followed for more than 18 months. Plast Reconstr Surg 2003;111:547–53.
[28] Stadelmann WK, Digenis AG, Tobin GR. Physiology and healing dynamics of chronic cutaneous wounds. Am J Surg 1998;176:26S–38S.
[29] Brown JR, Bromberg JH: preliminary studies on the effect of time–dose patterns in the treatment of keloids. Radiology 1963;80:298–300.
[30] Edsmyr F, Larsson LG, Onyango J, et al. Radiation therapy in the treatment of keloids in East Africa. Acta Radiol Ther Phys Biol 1974;13:102–6.
[31] Van Den Brenk HA, Minty CC. Radiation in the management of keloids and hypertrophic scars. Br J Surg 1960;47:595–605.
[32] Epstein Jr EH, Munderloh NH. Isolation and characterization of CNBr peptides of human $[\alpha 1(III)]_3$ collagen and tissue distribution of $[\alpha 1(I)]_2$–$\alpha 2$ and $[\alpha 1(III)]_3$ collagens. J Biol Chem 1975;250:9304–12.
[33] Hayakawa T, Hashimoto Y, Myokei Y, et al. Changes in type of collagen during the development of human postburn hypertrophic scars. Clin Chim Acta 1979;93:119–25.
[34] Cosman B, Wolff M. Bilateral earlobe keloids. Plast Reconstr Surg 1974;53:540–3.
[35] Hintz BL. Radiotherapy for keloid treatment. J Natl Med Assoc 1973;65: 71–5.
[36] Enhamre A, Hammar H. Treatment of keloids with excision and postoperative X-ray irradiation. Dermatologica 1983;167:90–3.

Please cite this article in press as: Sakamoto T et al. Dose–response relationship and dose optimization in radiotherapy ... Radiother Oncol (2009), doi:10.1016/j.radonc.2008.12.018

Radiol Phys Technol (2008) 1:171–177
DOI 10.1007/s12194-008-0024-3

Dose verifications by use of liquid ionization chamber of an electronic portal imaging device (EPID)

Kunihiko Tateoka · Atsushi Oouchi · Kensei Nakata · Masato Hareyama

Received: 22 November 2007 / Revised: 5 May 2008 / Accepted: 7 May 2008 / Published online: 7 June 2008

Abstract In this study, we examined the ability of an L-EPID to verify rectangular and irregular fields and to measure the transmitted exit doses. With respect to the beam profile of rectangular and irregular fields and the doses transmitted through an inhomogeneous phantom, the L-EPID dose obtained from the L-EPID measurement was compared with the conventional dose measured by use of a 0.12-cc ionization chamber and a 3D water phantom. In the comparison of the rectangular and irregular fields, the difference in the off-center ratio (OCR) between the L-EPID dose and the conventional dose was approximately 3% in the steep-dose-gradient region (penumbra regions, >30%/cm) and approximately ±0.5% in the gentle-dose-gradient region (5%/cm). On the other hand, the dose differences between the L-EPID and the measured doses were less than approximately 2% in the gentle-dose-gradient region. In addition, in the steep-dose-gradient region, the maximum difference was 30%. However, the differences in the distance-to-agreement (DTA) were less than approximately ±1 mm and were unrelated to the dose gradient. These results suggest that dose verification by L-EPID is very useful in clinical applications.

Keywords EPID · Photon dosimetry

K. Tateoka (✉) · M. Hareyama
Radiation Oncology, Imaging and Diagnosis,
Division of Organ Function and Therapeutics,
Molecular and Organ Regulation, Sapporo Medical University
Graduate School of Medicine, Sapporo 060-8556, Japan
e-mail: tateoka@sapmed.ac.jp

A. Oouchi · K. Nakata · M. Hareyama
Department of Radiology,
Sapporo Medical University School of Medicine,
Sapporo 060-8556, Japan

A. Oouchi
Department of Radiology, Teine Keijinkai Hospital,
Sapporo 006-8555, Japan

1 Introduction

In radiotherapy, image verification has been carried out by visual comparison of portal images with simulation images or digitally reconstructed radiographs (DRRs) generated from treatment planning systems (TPSs). Recently, images of electronic portal imaging devices (EPIDs) have been used instead of portal films for image verification. There are several types of EPID such as a mirror-based video system, a fiber-optic video system, a liquid ionization chamber system (L-EPID) [1], and an amorphous silicon system [2, 3]. Although the image collection methods are different in each system, image verification can be performed in a short time. Because EPID images are acquired with a computer on-line system, the acquisition is not interrupted by the process of developing films [4, 5]. On the other hand, in some methods, dose verification is performed by comparison of the calculated dose obtained from the TPS with the measured dose. Currently, the measured doses are acquired by use of semiconductor detectors attached to a body surface [6], and the exit doses transmitted by the human body are measured by the film method [7, 8]. However, when a semiconductor is used, the doses can be measured simultaneously at only a few points. Moreover, when the film method is used, considerable time is needed for developing the films. Therefore, it was generally considered that these methods were not satisfactory for clinical applications. For use of a dosimeter to measure the exit doses, the dosimetric characteristics of the

L-EPIDs have been studied by analysis of their image generating process [9–17].

As described previously in our theoretical study on the dosimetric characteristics of this device [9], we suggested the possibility of using the L-EPID as a dosimeter that can carry out dose verification.

In this article, we report the results of an actual dose verification performed by use of an L-EPID; we discuss the beam penumbra, flatness, symmetry, and off-center ratio (OCR) in rectangular and/or irregular fields, in addition to the verification of an exit dose transmitted through an inhomogeneous model phantom.

2 Instruments and methods

The L-EPID (Portal Vision system, Varian Medical Systems, Palo Alto, CA, USA) used in this study was equipped with a linear accelerator (CLINAC2100C, Varian Medical Systems) that generated voltages of 4 and 10 MV.

The ionization chamber was composed of a matrix of 256 × 256 pixels (total 65,536 pixels). The image collection area was 32.5 cm × 32.5 cm. Each pixel was 1.27 × 1.27 × 1.0 mm. The front and rear parts of the build-up region comprised approximately 10 and 5 mm of a water-equivalent material, respectively [10, 15]. For dose verification, we compared a calculated dose for the L-EPID (L-EPID dose) and a dose measured by use of a 3D water phantom scanning system (RFAplus, Scanditronix Wellhöfer, Germany) and a 0.12-cc ionization chamber (RK chamber, Scanditronix Wellhöfer).

The depth of the measurement point was fixed at the depth corresponding to the maximum dose (d_{max}) (4-MV X-rays: 1.0 cm; 10-MV X-rays: 2.5 cm). According to our previous report [9], water-equivalent solid phantoms (Tough Water™, Kyoto Kagaku Co., Ltd., Kyoto, Japan) with thicknesses of 3 and 18 mm were set on the L-EPID at X-ray energies of 4 and 10 MV, respectively. For matching the spatial resolution in measurements by using the RK chamber, a mean pixel value of 9 × 9 pixels was used as the L-EPID pixel value at arbitrary point. The variation in the L-EPID pixel value per single image was within approximately 0.5% of the standard deviation. Moreover, to reduce the variation, we used the average of the L-EPID pixel values of 10 images. Therefore, the variation in the average value is diminished to within 0.2% of the standard deviation. As described earlier, [9], within 15 s of image-collecting intervals, the L-EPID pixel values increased continuously in each image. On the basis of these results, we chose 30 s as the interval of image collection. The setting of the L-EPID and the accelerator is shown in Table 1.

Table 1 L-EPID conditions for 4-MV X-rays with 250 MU/min and 10-MV X-rays with 240 MU/min

Energy	4 MV	10 MV
Dose rate (MU/min)	250	240
Sync frequency (Hz)	400	180
Interpulse distance (ms)	2.50	5.56
HV row cycle time (ms)	12.50	11.11
Number of pulses used for on sync	5 pulses	2 pulses
Number of row per sync pulse	1 row	1 row
Number of averages (row sweeps)	2 scans	1 scan
Total acquisition time (s)	3.35	2.98

2.1 Sensitivity correction of L-EPID and dose conversion

The sensitivity compensation for each pixel in the L-EPID was performed according to the following process:

1. The energy of the X-rays and the dose rate are defined.
2. The detector is moved to the optional position (generally, the source-detector distance is 140 cm).
3. The EPID images are corrected without irradiation (dark image).
4. A large field in which all of the detection parts of the device are included was irradiated (flood image).

Each pixel value P (i and j) [16] in the L-EPID image was given by the following equation:

$$P(i,j) = [P^*(i,j) - B(i,j)] \times F^* / [F(i,j) - B(i,j)]. \quad (1)$$

where $P^*(i, j)$, $F(i, j)$, and $B(i, j)$ are the mean pixel values of the raw, flood, and dark images at the pixel numbers i and $J \cdot F^* = (i \times j)^{-1} \sum_{i=1}^{256} \sum_{j=1}^{256} [F(i,j) - B(i,j)]$ is the mean of all the pixel values in the flood image.

In this process, the X-ray outputs are supposed to be equal at arbitrary points in a "flood" field. However, the dose for the beam center axis is slightly lower than that for the off-center region because the actual X-rays generated from the accelerator are influenced by the field-flattening filter. Therefore, for obtaining an accurate L-EPID dose at the position of each pixel, the pixel value should be corrected with an output ratio at the respective pixel position versus the beam center axis (flood field correction, FFC). In the FFC method, Zhu et al. [16] assumed that the pixel values of the L-EPID are proportional to the square root of the dose. This relationship was reported by van Herk [12]. In addition, we have already reported that the pixel value of the L-EPID is proportional to the square root of the dose and also to the dose itself, and that it is very useful to introduce a correction factor that provides the daily deviation of the sensitivity of the ionization chambers of the L-EPID [9]. Therefore, at first we carried out the FFC

by using the OCR of the dose. If D_0 is the quantity of the dose for the central axis and $D_{i,j}$ is the dose for the off-axis corresponding to pixel numbers i and j, in the L-EPID, the correcting value $[F(i,j) - B(i,j)]^*$ for the flood image is expressed as follows:

$$[F(i,j) - B(i,j)]^* = D_0/D_{i,j}[F(i,j) - B(i,j)]. \quad (2)$$

If Eq. 2 is substituted in Eq. 1, the result is shown as

$$\overline{P(i,j)} = D_{i,j}/D_0 P(i,j). \quad (3)$$

Here, $\overline{P(i,j)}$ is the mean pixel value after the *FFC*.

For conversion to an L-EPID dose from pixel values, we use the following equation. Equation 4 has two new inserted terms for a revision to a theory of van Herk [12]. He had shown that pixel values vary directly as the square root of the irradiated dose, but we previously reported that pixel values are directly proportional to both the square root of the dose and the dose itself [9].

$$\overline{P(i,j)} = a \cdot D(i,j) + b \cdot \sqrt{D(i,j)} - k \cdot h[\cdot] \quad (4)$$

Here, $\overline{P(i,j)}$ is the pixel value; $D(i, j)$, the dose; a and b, constants; h, a sensitivity-correcting variable to express revisions such as the loss of ion recombination in an L-EPID ionization chamber, chronologic deviation of each pixel sensitivity, and saturation of electric charges depending on the collection interval; and k, the daily deviation factor. As shown in the earlier report [9], the coefficients were given as $a = 3.2381$, $b = 569.08$, and $h = 5.5168$ for 10-MV X-rays, and $a = 22.085$, $b = 260.32$, and $h = -0.1266$ for 4-MV X-rays. When the coefficients (a, b, and h) are previously defined, we can calculate k from two L-EPID images acquired on different days at the same measurement setting. The adopted conditions of measurement for determining k were as follows: The field size was 10 cm × 10 cm. The source–detector distance (SDD) was 100 cm, and the depth of the measurement point was d_{max}. In addition, the EPID pixel value was considered to be the mean value of 9 × 9 pixels on the central axis of a beam. Thus, the acquired k is 5.69 for 4-MV X-rays and 9.37 for 10-MV X-rays. The flood images and dose profiles used in the FFC were acquired previously. The flood image of the 40 cm × 40 cm field was collected at a depth d_{max} at an SDD of 100 cm. Subsequently, the dose profiles were determined by use of the RFAplus and the RK chamber.

2.2 Dose verification for rectangular and irregular fields

First, the beam symmetry, flatness, and penumbra (80 to 20%) of a 10 cm × 10 cm rectangular irradiation field were examined with an L-EPID. The L-EPID dose parameters were compared to the result of the measurement with the RFAplus phantom and RK chamber. In the next step, a multileaf collimator (each leaf had a thickness 1 cm at the isocenter plane) was used to form a 10 cm × 10 cm

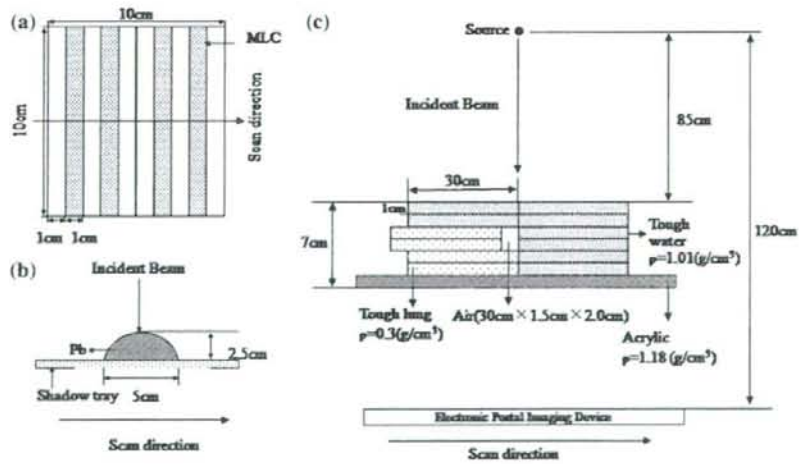

Fig. 1 Schematic diagrams of the irradiation setup. **a** Measurement of transmission dose with an irregular field by use of a multileaf collimator, and **b** cylindrical piece of lead (2.5 cm radius × 10 cm long, bisected lengthwise) on the shadow tray with a 10 cm × 10 cm field for 4- and 10-MV X-rays and a source-to-detector distance (SDD) of 100 cm. **c** Measurement of transmission dose with inhomogeneous phantom using water-equivalent solid phantom, lung-equivalent solid phantom, acrylic, and air with 10 cm × 10 cm field of 4- and 10-MV X-rays and an SDD of 120 cm

radiation field of alternating 1-cm-wide blocked and unblocked segments (Fig. 1a). The SDD was chosen to be 100 cm in this case.

2.3 Verification of exit dose transmitted to the inhomogeneous model phantom

As shown in Fig. 1b, we placed half of a cylindrical piece of lead (2.5 cm radius × 10 cm long, bisected lengthwise) on the shadow tray of the accelerator (Model 1).

The transmission dose was measured, and the dose distribution of a square field of size 10 cm × 10 cm for an SDD value of 100 cm was determined.

In the next step, we simulated a situation close, to a clinical situation by combined with a lung-equivalent solid phantom (Tough lung™, 30 cm × 30 cm, Kyoto Kagaku Co., Ltd., Kyoto, Japan), a water-equivalent solid phantom (Tough water™), and an atmosphere layer. Figure 1c shows the setting position of these phantoms (Model 2). The profiling of the exit dose in the above heterogeneous Model 2 was measured with a rectangular field size of 10 cm × 10 cm at an SDD of 100 cm.

3 Results

3.1 Sensitivity correction for L-EPID and dose conversion

Figure 2a shows the dose profile of a 40 cm × 40 cm field measured in the RK chamber for 4-MV X-rays. The dose increase compared to the central axis was observed to be approximately 2 and 5% at points at distances of ±3 and ±12 cm from the central axis, respectively. To study the usefulness of the FFC, two dose profiles of the rectangular field (10 cm × 10 cm) were calculated from the L-EPID measurement (before and after FFC use, respectively), and these dose distributions were compared against the measured distribution (Fig. 2). Before the FFC, a decrease in the L-EPID dose in the off-axis region was observed in comparison to the dose measured for the central axis. The maximum dose difference was approximately 4% in the gentle-dose-gradient area (distance from central axis less than ±4.5 cm, <5%/cm). On the other hand, it was approximately 3% in the steep-dose-gradient region (penumbra regions > 30%/cm). With regard to the distribution after the FFC, the difference between the L-EPID dose and the measured one in the steep-dose-gradient area was almost equal to the difference between the uncorrected L-EPID dose and the measured one. However, the difference was small (within approximately ±0.5%) in the gentle-dose-gradient region.

3.2 Dose verification for rectangular and irregular fields

Table 2 lists the symmetry, flatness, and penumbra from the post-FCC L-EPID dosimetry and the dose measured by use of the RK chamber. The differences in the symmetry

Table 2 Values of symmetry, flatness, and penumbra were calculated from the L-EPID dose obtained from the pixel values of the L-EPID and the dose in the water phantom at an SDD of 100 cm, a field size of 10 cm × 10 cm, and the maximum depth for 4-MV X-rays and 10-MV X-rays

	4 MV		10 MV	
	RK chamber	L-EPID	RK chamber	L-EPID
Symmetry (%)	1.30	1.29	1.40	1.60
Flatness (%)	1.20	1.21	1.60	1.80
Penumbra				
Right (mm)	6.20	6.00	7.60	7.50
Left (mm)	6.10	6.00	7.55	7.50

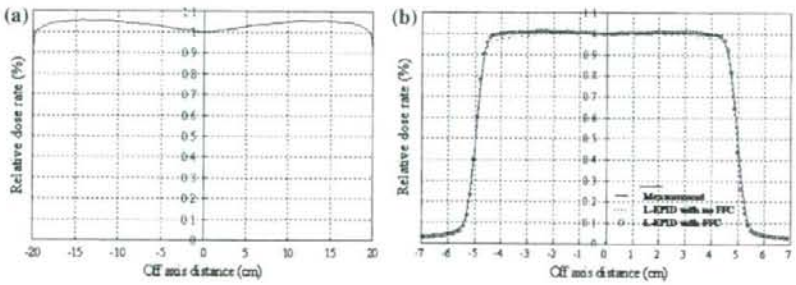

Fig. 2 **a** Off-center ratio of the dose in a water phantom at the maximum depth on the central axis for an SSD of 100 cm and a field size of 40 cm × 40 cm for 4-MV X-rays. **b** Comparison of off-center ratio between the L-EPID dose rates (*circles*) obtained from pixel values of the L-EPID, the dose (*line*) in a water phantom, and the L-EPID dose rates (*dotted line*) obtained from the pixel values of the L-EPID without correcting for the flood field correction at an SDD of 100 cm, a field size of 10 cm × 10 cm, and the maximum depth for 4-MV X-rays

between the L-EPID dose and the measured one were −0.1% for the 4-MV X-rays and 0.2% for the 10-MV X-rays. Similarly, the differences in flatness between the L-EPID dose and the measured dose were 0.01% for the 4-MV X-rays and 0.2% for the 10-MV X-rays; furthermore, the maximum penumbra was shown to be −0.2 mm for the 4-MV X-rays and −0.1 mm for the 10-MV X-rays.

Figure 3 shows the dose profiles obtained from the L-EPID dosimetry and the measurement with the RK chamber. Maximum discrepancies of approximately 8 and 5% were observed between the L-EPID and the measured doses for the 4-MV X-rays (a) and 10-MV X-rays (b), respectively.

3.3 Verification of exit dose transmitted through the model phantoms

The dose profiles obtained from the L-EPID measurement and the measurement with the RK chamber in Model 1 are shown in Fig. 4. The differences between the two profiles were observed to be approximately 25 and 10% for the 4-MV X-rays (a) and 10-MV X-rays (b) in the steep-dose-gradient region. However, in the gentle-dose-gradient region, the differences between them were within 0.5%. The dose distribution of the L-EPID dosimetry in Model 2 is shown in Fig. 5. The profiles were standardized at a point located at a distance of +2.0 cm from the central axis

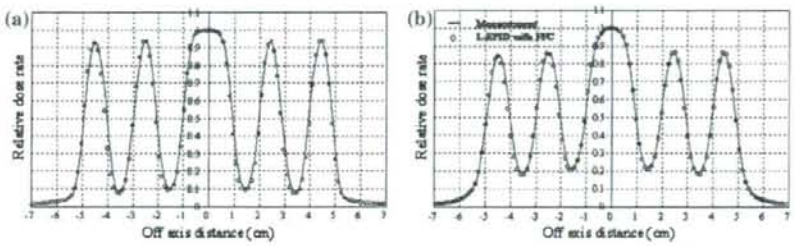

Fig. 3 Comparison of the off-center ratio of the irregular field between the L-EPID dose rates (*circles*) obtained from the pixel values of the L-EPID, the dose (*line*) in the water phantom at an SDD of 100 cm, a field size of 10 cm × 10 cm, and the maximum depth for 4-MV X-rays (a) and 10-MV X-rays (b)

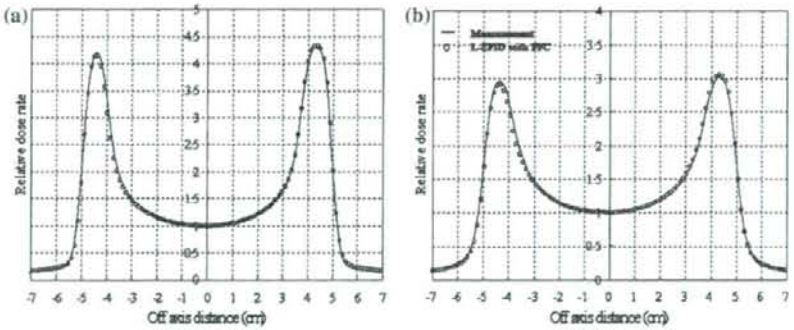

Fig. 4 Comparison of the off-center ratio of the transmission dose of the cylindrical piece of lead between the L-EPID dose rates (*circles*) calculated from the pixel values of the L-EPID at an SDD of 100 cm, and the dose (*line*) in the RK chamber at an SSD of 100 cm, field size of 10 cm × 10 cm, and the maximum depth for 4-MV X-rays (a) and 10-MV X-rays (b)

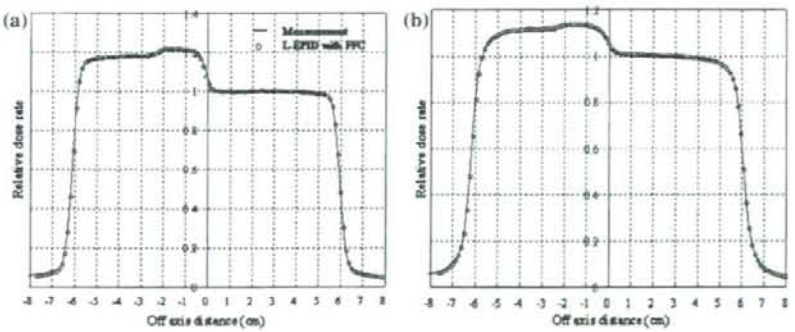

Fig. 5 Comparison of the off-center ratio of the transmission dose of the inhomogeneous phantom between the L-EPID dose rates (*circles*) obtained from the pixel values of the L-EPID and the dose rates (*line*) in the RK chamber at an SDD of 100 cm, a field size of 10 cm × 10 cm, and the maximum depth for 4-MV X-rays (a) and 10-MV X-rays (b)